arXiv:2605.10747v1 [cond-mat.mes-hall] 11 May 2026

Theory of Spin-splitter Magnetoresistance in Altermagnets

Tim Kokkeler *
Department of Physics and Nanoscience Center, University of Jyväskylä, P.O. Box 35 (YFL), FI-40014 University of Jyväskylä, Finland

Vitaly N. Golovach
Centro de Física de Materiales (CFM-MPC) Centro Mixto CSIC-UPV/EHU, E-20018 Donostia-San Sebastián, Spain Donostia International Physics Center (DIPC), 20018 Donostia-San Sebastián, Spain and IKERBASQUE, Basque Foundation for Science, 48013 Bilbao, Spain

F. Sebastian Bergeret
Centro de Física de Materiales (CFM-MPC) Centro Mixto CSIC-UPV/EHU, E-20018 Donostia-San Sebastián, Spain and Donostia International Physics Center (DIPC), 20018 Donostia-San Sebastián, Spain

We develop a theory of angle-dependent magnetoresistance (ADMR) in metallic altermagnets coupled to ferromagnetic insulators and establish criteria that distinguish them from conventional compensated magnets with spin–orbit coupling. We show that the spin-splitter magnetoresistance (SSMR) reported by H. Chen *et al.* [*Adv. Mater.* **37**, 2507764 (2025)] constitutes a smoking-gun signature of collinear altermagnetism in metallic systems. In contrast to spin-Hall magnetoresistance (SMR), SSMR exhibits three key distinctions: it depends solely on the relative orientation between the ferromagnetic magnetization and the altermagnetic Néel vector, yields a longitudinal ADMR response of opposite sign, and features a direct proportionality between longitudinal and transverse ADMR signals, absent in SMR. These results provide a clear route to unambiguously identify altermagnets in transport.

Altermagnets, a recently introduced class of magnetic materials [1, 2], have rapidly become a central topic following their theoretical prediction. Extensive work has identified their distinctive signatures [3–17], and experiments have reported evidence of altermagnetism in several materials [18–23]. Altermagnets combine defining features of both ferromagnets and antiferromagnets while remaining distinct from either: despite a fully compensated magnetic structure with zero net magnetization, they host a pronounced spin-dependent electronic structure dictated by crystal symmetry rather than spin–orbit coupling. This yields large momentum-dependent spin splittings, enabling robust spin polarization and anisotropic transport without macroscopic magnetization. Altermagnets thus establish a platform for spin transport that is intrinsically resilient to external magnetic fields.

Altermagnets are symmetry-distinct from conventional antiferromagnets. While conventional antiferromagnets are invariant under the combined action of time reversal $\mathcal{T}$ with translation t or inversion $\mathcal{P}$, altermagnets require an additional rotation $\mathcal{R}$—that is, they are invariant under $\mathcal{TR}$, $\mathcal{TR}t$, or $\mathcal{TRP}$ [1]. This symmetry distinction has direct electronic consequences. Collinear antiferromagnets with $\mathcal{TP}$ symmetry exhibit no spin splitting, whereas noncollinear antiferromagnets lacking this symmetry can display odd-in-momentum spin splitting, as in p-wave magnets [24, 25]. In contrast, altermagnets exhibit even-in-momentum spin splitting. Being nonrelativistic in origin, this splitting can be large, enabling efficient charge–spin interconversion via the spin-splitter effect and its inverse [7, 9, 12–17], as well as other recently reported transport effects [26, 27].

These phenomena can be explored using magnetoresistance (MR) measurements, which constitute a central class of spin-dependent transport probes in magnetic systems. By linking electrical resistance to magnetic configuration, spin-dependent scattering, and spin–orbit coupling, MR provides a powerful probe of magnetic order and spin–charge interconversion. Prominent examples include anisotropic magnetoresistance (AMR) [28], giant magnetoresistance (GMR) [29–31], tunnel magnetoresistance (TMR) [6, 32], Hanle magnetoresistance (HMR) [33, 34], and spin-Hall magnetoresistance (SMR) [35–45]. The latter two constitute hallmark signatures of the spin Hall effect in heavy-metal systems.

In this Letter, we address whether altermagnets can be distinguished from conventional compensated magnets via MR measurements. We develop a theory of angle-dependent magnetoresistance (ADMR) in metallic d-wave altermagnets coupled to a magnetic insulator, a bilayer geometry recently explored experimentally in Ref. [23]. We show that the spin-splitter magnetoresistance (SSMR) reported in Ref. [23] provides a hallmark signature of altermagnetism, provided the full set of angular dependencies is probed.

While SSMR was originally introduced in close analogy to SMR, with the spin Hall angle replaced by the spin-splitter mechanism, we find that it differs qualitatively from SMR. As a nonrelativistic effect, SSMR is expected to yield larger signals than SMR and, more importantly, exhibits distinct transport signatures. In particular, the longitudinal response displays an angular dependence op-

* tim.h.kokkeler@jyu.fi

posite to that of SMR, while the transverse resistance is directly proportional to the longitudinal correction, in contrast to SMR. These features establish SSMR as a distinct class of ADMR, separate from spin–orbit-driven magnetoresistance such as SMR and HMR, and identify it as a powerful probe of altermagnetism.

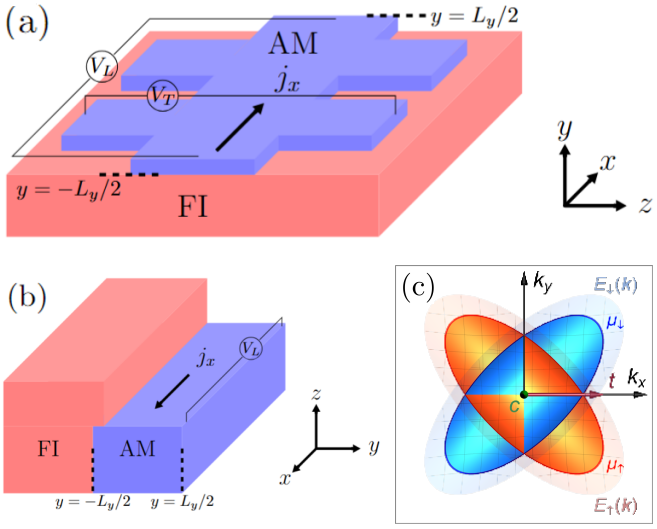

FIG. 1. Two setups suitable for SSMR measurements. In both cases, a collinear altermagnet (AM), is coupled to a ferromagnetic insulator (FI) and driven by a charge current (j_x). This charge current induces a spin current and therefore a spin accumulation near the interface, with spin along the Néel vector. This spin in turn via the inverse effect, modifies the charge current. The FI can rotate or absorb this spin, thereby influencing the effectiveness of this process. This affects charge transport within the system, which can be detected via voltage probes $V_{L,T}$. The side-coupled geometry shown in (b) additionally enables measurement of the transverse SSMR response. (c) Top view of the band structure of a d-wave altermagnet: the altermagnetic "flower" arises from the intersection of the spin-split bands $E_\uparrow$ and $E_\downarrow$, filled up to chemical potentials $\mu_\uparrow$ and $\mu_\downarrow$. The spin-splitter vector t_i and the crystal c-axis c_i define the orientation of the spin-splitter tensor T_{ij} [Eq. (7)].

We consider the setups shown in Fig. 1, consisting of a collinear altermagnet (AM) with Néel vector N_a in contact with a ferromagnetic or ferrimagnetic insulator (FI) at $y = -L_y/2$. To describe charge and spin dynamics, we employ the kinetic equations [7]:

$$\partial_t \delta n + \partial_k j_k = 0, \tag{1}$$

$$\partial_t \delta S_a + \partial_k j^s_{ka} = -\Gamma_{ab}\delta S_b, \tag{2}$$

where δn and $\delta \boldsymbol{S}$ denote the excess charge and spin densities, with j_k and j^s_{ka} their associated fluxes, and Γ_{ab} is the spin-relaxation tensor. In collinear altermagnets,

$$\Gamma_{ab} \;=\; \tau^{-1}_{s\perp}(\delta_{ab} - N_a N_b) + \tau^{-1}_{s\parallel} N_a N_b, \tag{3}$$

with $\tau_{s\parallel}$ and $\tau_{s\perp}$ the relaxation times for spin components parallel and perpendicular to the Néel vector. These

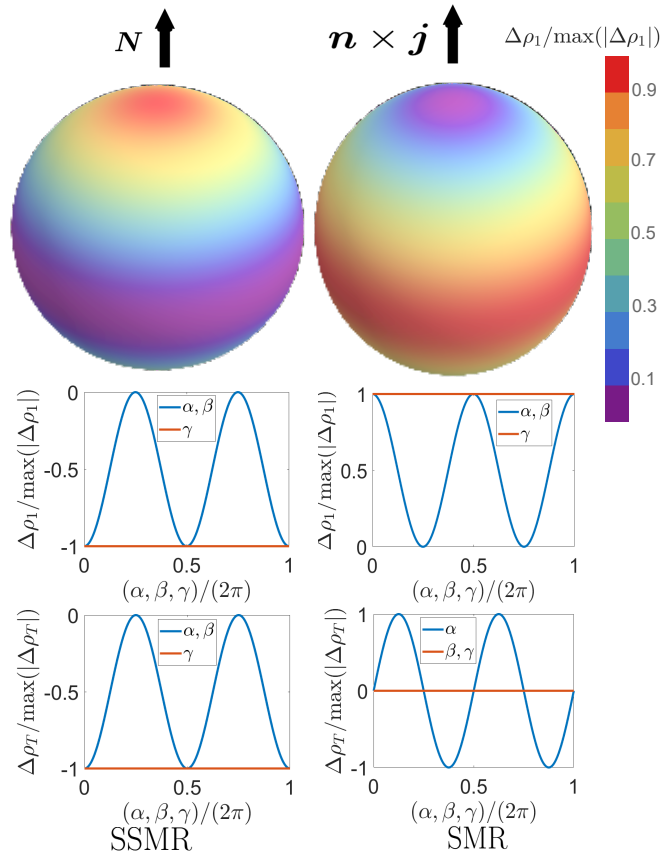

FIG. 2. The longitudinal MR $\Delta\rho_1$ (top and middle row) and transverse MR $\Delta\rho_T$ (bottom row) as a function of angle of the magnetization for the SSMR (left) and SMR (right). The polar axis corresponds to the direction of the Néel vector for the SSMR, and to the cross-product of the normal to the interface and the direction of the current for the SMR. *Top row:* For the SMR [36], the resistance is maximized at the polar axis and minimized in the plane perpendicular to the polar axis, while for the SMR exactly the opposite holds. Results have been normalized using the maximum absolute value. *Middle row:* Line cuts around the surface of the sphere, with the angles α, β, γ corresponding to the convention from SMR [46]. *Bottom row:* For the SSMR the angle dependence of the transverse resistance is identical to that of the longitudinal resistance, while for the SMR it is qualitatively different [36].

times generally differ: the altermagnetic band splitting couples to transverse spins while leaving the longitudinal component largely unaffected. The transverse spin therefore undergoes efficient dephasing due to inhomogeneous broadening arising from the momentum dependence of the altermagnetic splitting $E_\uparrow(\boldsymbol{k}) - E_\downarrow(\boldsymbol{k})$, where $\boldsymbol{k}$ is the electron wave vector. For a planar d-wave splitting $E_\uparrow(\boldsymbol{k}) - E_\downarrow(\boldsymbol{k}) = 4\hbar J k_x k_y / k_F^2$ [47] perturbatively taken into account for electrons on a spherical Fermi surface $|\boldsymbol{k}| = k_F$ in 3D, the variance of the precession frequency is $\langle \delta\omega^2 \rangle = (16/15)J^2$, yielding a dephasing time $\sim 1/J$, set by the band-splitting scale J. This regime corre-

sponds to very clean systems with momentum relaxation time $\tau_p \gtrsim 1/J$, where Eq. (2) applies only in the limit $\tau_{s\perp} \approx 0$ and for times much longer than τ_p. In contrast, $\tau_{s\parallel}$ remains long ($\tau_{s\parallel} \gg \tau_p$), being limited by spin–orbit scattering from residual disorder.

In disordered systems ($\tau_p J \ll 1$), motional narrowing leads to

$$\frac{1}{\tau_{s\perp}} = \frac{1}{\tau_{s\parallel}} + \alpha \tau_p J^2, \tag{4}$$

with $\alpha = 16/15$ for the 3D model above and $\alpha = 2$ in 2D. This regime bears some resemblance to the Dyakonov–Perel mechanism, although here the effect originates from fluctuations of the precession frequency without randomization of the precession axis [17, 48, 49]. We note that Eq. (4) contains no interference terms between spin–orbit scattering and altermagnetic splitting fluctuations, owing to their different parity in $\boldsymbol{k}$.

For d-wave altermagnets, the charge and spin current densities entering Eqs. (1) and (2) read [7]:

$$j_k = \frac{\sigma}{e}\left(\partial_k \mu + \frac{1}{2} N_a T_{kj} \partial_j \mu_a^s\right), \tag{5}$$

$$j_{ka}^s = -\frac{\hbar\sigma}{4e^2}\left(\partial_k \mu_a^s + 2N_a T_{kj}\partial_j \mu + \varepsilon_{abc} N_b K_{kj} \partial_j \mu_c^s\right), \tag{6}$$

where $\sigma = 2e^2\nu_0 D$ is the Drude conductivity, e is the elementary charge, ν_0 is the density of states per spin ($\nu_\uparrow = \nu_\downarrow \equiv \nu_0$), D is the diffusion constant at the Fermi level, and ε_{abc} is the Levi-Civita symbol. The mean chemical potential is defined as $\mu = (\mu_\uparrow + \mu_\downarrow)/2$ and the spin bias as $\boldsymbol{\mu}^s = 2\delta \boldsymbol{S}/(\hbar\nu_0)$, such that $\boldsymbol{N}\cdot\boldsymbol{\mu}^s = \mu_\uparrow - \mu_\downarrow$, where $\mu_\uparrow$ and $\mu_\downarrow$ denote the chemical potentials of the spin-up and spin-down bands. Altermagnetism in Eqs. (5) and (6) is encoded in two symmetric tensors: (i) the spin-splitter tensor T_{jk} [7, 50–61], which couples charge and spin degrees of freedom, and (ii) the spin-swap tensor K_{jk}, analogous to the spin-swapping term in the spin Hall effect [62], which affects spin currents with polarization perpendicular to the Néel vector. In collinear systems, K_{jk} does not contribute directly to the charge current [7] and will be neglected in the following.

The spin-splitter tensor T_{ij} is fixed by crystal symmetry. For a planar d-wave altermagnet with parabolic dispersion, it takes the form

$$T_{ij} = \frac{2\hbar J}{E_F}\left(t_i \varepsilon_{jkl} + t_j \varepsilon_{ikl}\right) c_k t_l, \tag{7}$$

where E_F is the Fermi energy and $\boldsymbol{t}$ and $\boldsymbol{c}$ are unit vectors along the direction of maximal spin-splitter response and the crystallographic c-axis, respectively [see Fig. 1(c)]. This tensor encodes the spin-splitter effect: spin-up and spin-down carriers are deflected anisotropically, generating a transverse spin current polarized parallel to $\boldsymbol{N}$. Although $\boldsymbol{N}$ can be reoriented by external fields or torques, $\boldsymbol{t}$ and $\boldsymbol{c}$ are rigidly fixed by the lattice. Consequently, the spin-splitter response depends strongly on the crystallographic orientation.

Spin accumulation at the interface vanishes completely when the interface is perpendicular to the c-axis, as well as in the more general geometries where the interface plane contains either of the vectors $\boldsymbol{t}+\boldsymbol{c}\times\boldsymbol{t}$ or $\boldsymbol{t}-\boldsymbol{c}\times\boldsymbol{t}$. In contrast, the accumulation is maximal when the charge current is aligned with one of the vectors $\boldsymbol{t}$ or $\boldsymbol{c}\times\boldsymbol{t}$ and the interface normal is parallel to the remaining vector.

Figure 1(a) depicts the Hall-bar geometry with a FI at the bottom interface, as typically used in SMR experiments. Here the altermagnet is oriented such that its d-wave "flower" optimally generates spin accumulation at the top and bottom interfaces. Notably, (101)-oriented epitaxial RuO_2 thin films were employed in Ref. [23] precisely to produce a misalignment between the altermagnetic "flower" and the film plane. While such non-c-axis epitaxial growth is readily achieved in many rutile oxides via substrate templating, it may not be feasible for all altermagnets—especially strictly two-dimensional systems. In those cases, the lateral-coupling geometry shown in Fig. 1(b) provides a practical alternative. The results presented below apply to both configurations.

We compute the longitudinal and transverse resistances as functions of the FI magnetization direction by solving the transport equations with appropriate boundary conditions. At the vacuum interface ($y = L_y/2$), the normal components of the charge and spin currents vanish. At the AM/FI interface ($y = -L_y/2$), the charge current is set to zero, while the spin current satisfies [36, 45, 63, 64]

$$\frac{2e^2}{\hbar}\boldsymbol{j}_y^s = G_i \boldsymbol{m}\times\boldsymbol{\mu}^s + G_r \boldsymbol{m}\times(\boldsymbol{m}\times\boldsymbol{\mu}^s) - |G_s|\boldsymbol{\mu}^s, \tag{8}$$

where $\boldsymbol{m}$ is the unit vector along the FI magnetization and the vector notation refers to spin space. As in SMR, the interface is parametrized by the spin-mixing conductance $G_{\uparrow\downarrow} = G_r + iG_i$ and the spin-sink conductance $G_s < 0$. These parameters depend on temperature and magnetic field [45] and are sensitive to the magnetic state of the FI and interfacial disorder.

We consider the linear response to a stationary, homogeneous charge-current density j_x in the geometries of Figs. 1(a) and (b). We retain the transport coordinate frame shown in the figures while allowing an arbitrary crystal-lattice orientation, further considering a generic spin-splitter tensor T_{ij}. Translational invariance requires the chemical potential and spin bias to take the form $\mu = -Ex + \delta\mu(y)$ and $\partial_x \mu^s = 0$, where E is the uniform x-component of the electric field. With this ansatz, the continuity equations (1) and (2), together with the currents in Eqs. (5) and (6), reduce to an effective one-dimensional problem. Averaging the current density over the film thickness then yields $\bar{j}_x = \sigma E + \delta\bar{j}$, with

$$\delta\bar{j} = -\frac{\sigma T_{xy}}{2eL_y}\boldsymbol{N}\cdot\left[\boldsymbol{\mu}^s\left(\frac{L_y}{2}\right) - \boldsymbol{\mu}^s\left(-\frac{L_y}{2}\right)\right]. \tag{9}$$

This expression closely resembles the SMR, except that the role of the spin Hall angle is played by the tensor component T_{xy} and the spin accumulation enters solely through its projection onto $\boldsymbol{N}$. The same projection governs the transverse current j_z, which obeys the simple proportionality

$$\bar{j}_z = \frac{T_{yz}}{T_{xy}} \delta \bar{j}. \tag{10}$$

This relation stands in stark contrast to the spin Hall effect (and related phenomena such as SMR and HMR), where the longitudinal and transverse responses depend on independent components of the spin accumulation (μ_z and μ_x, respectively) rather than on the single combination $\boldsymbol{N} \cdot \boldsymbol{\mu}^s$. Consequently, the ADMR of the SSMR differs markedly from that of SMR when both the longitudinal and transverse signals are measured.

For the longitudinal (ρ_L) and transverse (ρ_T) resistivities, we obtain (see Appendix A)

$$\rho_L = \sigma^{-1} + \Delta\rho_L \quad \text{and} \quad \rho_T = \frac{T_{yz}}{T_{xy}} \Delta\rho_L, \tag{11}$$

where

$$\Delta\rho_L = \frac{2T_{xy}^2 l_{s_\parallel}}{\sigma L_y} \tanh\left(\frac{L_y}{2l_{s\parallel}}\right) \frac{\sigma + |G_s| l_{s\parallel} \coth\left(\frac{L_y}{2l_{s\parallel}}\right) + \bar{G}\left[l_{s\parallel} \coth\left(\frac{L_y}{2l_{s\parallel}}\right) - 2l_{s\perp} \coth\left(\frac{L_y}{l_{s\perp}}\right)\right] \sin^2\phi}{\sigma + 2|G_s| l_{s\parallel} \coth\left(\frac{L_y}{l_{s\parallel}}\right) + 2\bar{G}\left[l_{s\parallel} \coth\left(\frac{L_y}{l_{s\parallel}}\right) - l_{s\perp} \coth\left(\frac{L_y}{l_{s\perp}}\right)\right] \sin^2\phi}, \tag{12}$$

with spin-relaxation lengths $l_{s\parallel,\perp} = \sqrt{D\tau_{s\parallel,\perp}}$, angle ϕ between $\boldsymbol{N}$ and $\boldsymbol{m}$, and effective spin-mixing conductance

$$\bar{G} = \mathrm{Re} \frac{G_{\uparrow\downarrow}}{1 + \frac{2l_{s\perp}}{\sigma}\left(|G_s| + G_{\uparrow\downarrow}\right) \coth\left(\frac{L_y}{l_{s\perp}}\right)}. \tag{13}$$

Equations (11) and (12) constitute the central result of this work. They describe the ADMR of the AM/FI structures in Fig. 1 and establish the theoretical framework for future SSMR experiments.

For $l_{s\parallel} = l_{s\perp}$, the ADMR is harmonic:

$$\rho_L = \sigma^{-1} + \Delta\rho_0 + \Delta\rho_1 \left[1 - (\boldsymbol{m} \cdot \boldsymbol{N})^2\right], \tag{14}$$

$$\rho_T = \frac{T_{yz}}{T_{xy}} \left\{\Delta\rho_0 + \Delta\rho_1 \left[1 - (\boldsymbol{m} \cdot \boldsymbol{N})^2\right]\right\}, \tag{15}$$

where

$$\Delta\rho_0 = \frac{2T_{xy}^2 l_s}{\sigma L_y} \frac{\sigma \tanh\left(\frac{L_y}{2l_s}\right) + |G_s| l_s}{\sigma + 2|G_s| l_s \coth\left(\frac{L_y}{l_s}\right)}, \tag{16}$$

$$\Delta\rho_1 = -\frac{2T_{xy}^2 l_s}{\sigma L_y} \frac{\bar{G} l_s \tanh^2\left(\frac{L_y}{2l_s}\right)}{\sigma + 2|G_s| l_s \coth\left(\frac{L_y}{l_s}\right)}. \tag{17}$$

Here, Eq. (18) resembles the ADMR of SMR [36, 45], expect that the corrections in Eqs. (16) and (17) are of opposite sign.

For $l_{s\parallel} = l_{s\perp}$ the results can be written in a form very similar to the SMR results [36, 45]:

$$\rho_L = \rho_0 + \Delta\rho_0 + \Delta\rho_1 (1 - (\boldsymbol{m} \cdot \boldsymbol{N})^2) \tag{18}$$

$$\rho_T = \frac{T_{yz}}{T_{xy}} \left(\Delta\rho_0 + \Delta\rho_1 (1 - (\boldsymbol{m} \cdot \boldsymbol{N})^2)\right), \tag{19}$$

where

$$\frac{\Delta\rho_0}{\rho_0} = 2T_{xy}^2 \frac{l_s}{L_y} \frac{\tanh\left(\frac{L_y}{2l_s}\right) + \frac{|G_s| l_s}{\sigma}}{1 + \frac{2|G_s| l_s}{\sigma} \coth\frac{L_y}{l_s}}, \tag{20}$$

$$\frac{\Delta\rho_1}{\rho_0} = -T_{xy}^2 \frac{l_s}{L_y} \tanh^2\left(\frac{L_y}{2l_s}\right) \frac{2\bar{G} l_s}{\sigma + 2G_s l_s \coth\frac{L_y}{l_s}}. \tag{21}$$

The longitudinal resistivity contains two corrections. $\Delta\rho_0$ is independent of the direction of the magnetization, and therefore it is difficult to measure. On the other hand, $\Delta\rho_1$ depends on the direction of $\boldsymbol{m}$. It thus gives an MR effect. The effect requires a nonzero spin-mixing conductance $G_{\uparrow\downarrow}$, while the spin-sink conductance G_s reduces the effect.

To compare the SSMR and SMR [36] we show the angle dependence of the longitudinal MR in Fig. 2. There are three marked differences between the SSMR and SMR. First of all, there is a sign difference between the two contributions. Indeed, while the SMR resistance is maximized along a particular axis and minimized in the plane perpendicular to this axis, the SSMR is minimized along a certain axis and maximized in the plane perpendicular to it. This difference is due to the fact that the altermagnet tensor T_{jk} is symmetric in its indices, so that $T_{xy}T_{yx} = T_{xy}^2 > 0$, while the spin-Hall tensor θ_{ajk} is antisymmetric so that $\theta_{zxy}\theta_{zyx} = -\theta_{zxy}^2 < 0$. This means that the SSMR and the SMR can be directly distinguished by considering the dependence of the resistance on the magnetization direction, as illustrated in Fig. 2. Negative SMR signals have also been discussed for systems in heavy metal antiferromagnetic insulator hybrids. This was explained by a tendency of the Neel vector to orient perpendicular to the magnetic field [65–71]. However, since this is a property of the insulator

rather than the metal, such effects can be clearly distinguished from the SSMR effect.

A second difference between the SSMR and SMR is that for SSMR the spin quantization axis is uniquely determined by the direction of the Néel vector. This difference stems from the fact that the altermagnet tensor $N_a T_{jk}$ can be written as a direct product of the Néel vector and a real space tensor, while this is not possible for the spin-Hall tensor $\theta\varepsilon_{ajk}$ in which all indices are coupled. This feature can be detected experimentally in four-probe setups.

Thirdly, the transverse resistance is distinctly different for the SSMR and the SMR. Indeed, within the SSMR the transverse resistance is directly proportional to the correction of the longitudinal resistance and thus has the same magnetic field dependence. On the other hand, in the SMR the transverse and longitudinal resistances have distinctly different angle dependence [36]. Also this difference traces back directly to the fact that the altermagnet tensor is a direct product of the Néel vector and a real space tensor, so that the longitudinal and transverse response are determined by the same component of spin accumulation, $\boldsymbol{N}\cdot\boldsymbol{\mu}^s$, while in the SMR the longitudinal and transverse responses are determined by different components of the spin-accumulation.

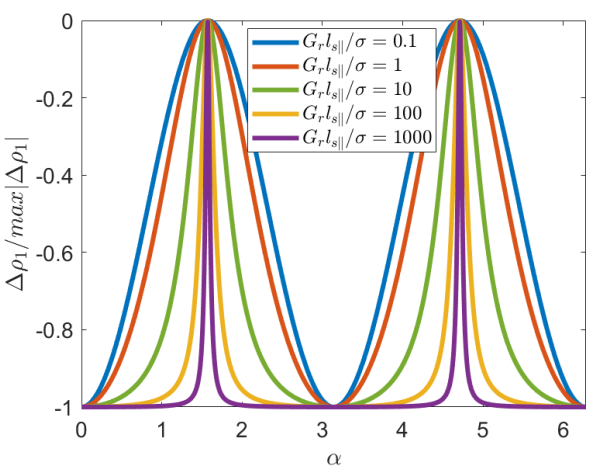

FIG. 3. The angle (α) dependence of the resistivity in an altermagnet with strong relaxation for spins not along the Néel vector, where $\Delta\rho_1(\alpha) = \Delta\rho(\alpha) - \Delta\rho(\frac{\pi}{2})$. For large $G_r l_{s\|}/\sigma$ the signal strongly deviates from the usual harmonic form, instead showing narrow dips within broad plateaus. We used $G_s = 0$ and assumed $L_y \gg l_s$.

A fourth feature that distinguishes the SSMR from the SMR is revealed by considering different Hall bars which are related via a 90 degrees rotation and are located on the same domain of the altermagnet. Indeed, the spin-Hall effect is isotropic, so rotation symmetry dictates the longitudinal resistance should be the same in both bars, while the transverse resistance has opposite sign. On the other hand, for SSMR, the longitudinal resistivities of the bar are proportional to T_{xy}^2 and T_{yz}^2 respectively and therefore they do not necessarily have the same magnitude. The transverse resistivities on the other hand are both proportional to $T_{yz}T_{yz}$, so that they are equal. Thus, an additional tool to distinguish SSMR from SMR is by comparing the longitudinal and transverse resistivities of different Hall bars.

While useful to make the connection with the SMR effect, in a realistic altermagnet spin relaxation is highly anistropic, spins perpendicular to the collinear axis relax much faster than those along the collinear axis. To illustrate the effect of such anisotropy, we consider the limit $l_{s\perp} \ll l_{s\|}$. Moreover, for many interfaces, dephasing, which appears naturally due to the precession phase in scattering processes, is much more important than spin-flip processes, which require energy exchange, for example through magnons. Since G_s only contains contributions from spin-flip processes while G_r contains contributions of both processes [45], for many interfaces $|G_s| \ll G_r$. In this limit, the SSMR possesses an elegant structure:

$$\frac{\Delta\rho}{\rho} = -\frac{2T_{xy}^2 l_{s\|}}{L_y}\left(\frac{\sigma + G_r l_{s\|}(1-(\boldsymbol{m}\cdot\boldsymbol{N})^2)\coth\frac{L_y}{2l_{s\|}}}{\sigma + 2G_r l_{s\|}(1-(\boldsymbol{m}\cdot\boldsymbol{N})^2)\coth\frac{L_y}{l_{s\|}}}\right). \tag{22}$$

The qualitative features discussed before remain the same in this limit. However, there are also a few differences. In contrast to the isotropic relaxation limit, the magnetoresistance is not harmonic, the denominator contains additional angle dependence. The relative importance of this angle dependence depends on the bulk conductivity, as illustrated in Fig. 3. In the high conductivity limit $G_r l_{s\|}/\sigma \ll 1$ the anharmonicity effects are small. However, in the limit of low conductivity of the altermagnet, $G_r l_{s\|}/\sigma \gg 1$, resistivity has narrow dips around angles for which m is parallel or antiparallel to $\boldsymbol{N}$. As shown in Appendix B, anisotropic relaxation has the opposite effect on the SMR in antiferromagnets, the peaks become broader and the dips become sharper. This shows that in the low conductivity limit the anharmonicity can be used to pinpoint anisotropic relaxation. Additionally, Eq. (22) contains only the real part G_r of the spin-mixing conductance, while the imaginary part G_i drops out completely. This illuminates the need to use FIs that result in an interface with large G_r.

So far, we have compared SSMR in altermagnets with SMR in normal metals. In order to distinguish altermagnets from antiferromagnets, it is imperative to compare SSMR with the SMR in such materials instead. The SMR in antiferromagnets has features of both the SMR in normal metals and of the SSMR. Indeed, as shown in Appendix B, like for the SSMR, the resistance of the SMR in antiferromagnets depends on the angle between the magnetization of the FI and the Néel vector and the transverse and longitudinal resistivities have the same angle dependence. Moreover, like in SSMR, anisotropic relaxation leads to an anharmonicity due to the appearance of $1-(\boldsymbol{N}\cdot\boldsymbol{m})^2$ not only in the numerator, but

Effect	Sign	Axis	Anharmonicity	Magnitude
SMR in NM	+	$\boldsymbol{n}\times\boldsymbol{j}$	✗	θ^2
SMR in AFM	+	$\boldsymbol{N}$	✓	$\theta^2(\boldsymbol{N}\cdot(\boldsymbol{n}\times\boldsymbol{j}))^2$
SSMR	-	$\boldsymbol{N}$	✓	T_{xy}^2

TABLE I. Comparison of SMR in normal metals (NM) and antiferromagnets (AFM) to the SSMR introduced here. By considering the sign of the effect, the axiality, anharmonicity and magnitude, the three effects can be distinguished.

also in the denominator. On the other hand, the sign of SMR for antiferromagnets is the same as for the SMR for normal metals and thus opposite to SSMR. Moreover, this sign difference means that the anharmonicity leads to a widening of the peaks and tightening of the dips, contrary to the SSMR. Moreover, the magnitude of the effect is determined by the relative direction of $\boldsymbol{N}$ and $\boldsymbol{n}\times\boldsymbol{j}$. This shows that the SMR in antiferromagnets can be easily distinguished both from the usual SMR and from the SSMR.

In conclusion, we have uncovered a new type of ADMR, the SSMR. While the SSMR bears similarities with the SOC-induced SMR, we highlighted several differences that can be used to distinguish the two. We have shown that an extension of the experimental studies in Ref. [23] that includes the entire angle dependence of the longitudinal and transverse ADMR can be used to unambiguously detect the existence of a d-wave spin-splitting, a hallmark of d-wave altermagnetism.

Magnetic insulators as those used in SMR, such as YiG [46] or EuS [72] may serve to test our predictions. We recommend to ensure that the preferred magnetization direction of the ferromagnetic insulator is much softer than the preferred Néel vector direction of the altermagnet, and to use weak fields, to reduce the reorientation of the Néel vector in the presence of magnetic fields. Another important design criterion stems from the fact that all altermagnets except those of the $^{2}2/^{2}m$ spin space group [7, 53] have planar altermagnetism, i.e. there is a 2D altermagnet d-wave order. In this case, denoting the angle between the normal of the AM/FI interface and the altermagnet planes by δ, since $T_{xy}\sim\sin\delta$, the effect scales as $\sin^2\delta$. This provides constraints on the optimal surface direction for the effect. In addition to the SSMR, a real altermagnet also displays the AMR, SMR and HMR effects. However, since SMR is relativistic and AMR and HMR strongly depend on the strength of the external magnetic field while in SSMR the magnetic field is only needed to rotate the magnetization of the FI, we expect that the SSMR is dominant in the low-field regimes, as is the case for SMR effects [45].

I. ACKNOWLEDGMENTS

We thank Tero Heikkilä for useful discussions. T. K. acknowledges support by the Research Council of Finland through DYNCOR, Project Number 354735 and through the Finnish Quantum Flagship, Project Number 359240. Moreover, his work is part of the Finnish Centre of Excellence in Quantum Materials (QMAT). F. S. B. thanks financial support from the the Spanish MCIN/AEI/10.13039/501100011033 through the grant PID2023-148225NB-C31, and the European Union's Horizon Europe research and innovation program under grant agreement No. 101130224 (JOSEPHINE). V.N.G. acknowledges funding from the Spanish MCIN/AEI/10.13039/501100011033 through grant PID2024-160189NA-I00, co-funded by the European Regional Development Fund (FEDER, EU), as well as from the Basque Government through grants PIBA_2025_1_0018, IT-1591-22, and IKUR/RESONANT.

[1] L. Šmejkal, J. Sinova, and T. Jungwirth, Phys. Rev. X **12**, 040501 (2022).
[2] T. Jungwirth, R. M. Fernandes, J. Sinova, and L. Smejkal, arXiv preprint arXiv:2409.10034 10.48550/arXiv.2409.10034 (2024).
[3] R. Zarzuela, R. Jaeschke-Ubiergo, O. Gomonay, L. Šmejkal, and J. Sinova, Phys. Rev. B **111**, 064422 (2025).
[4] M. Leiviskä, J. Rial, A. Bad'ura, R. L. Seeger, I. Kounta, S. Beckert, D. Kriegner, I. Joumard, E. Schmoranzerová, J. Sinova, O. Gomonay, A. Thomas, S. T. B. Goennenwein, H. Reichlová, L. Šmejkal, L. Michez, T. c. v. Jungwirth, and V. Baltz, Phys. Rev. B **109**, 224430 (2024).
[5] Q. Cheng, Y. Mao, and Q.-F. Sun, Phys. Rev. B **110**, 014518 (2024).
[6] F. Liu, Z. Zhang, X. Yuan, Y. Liu, S. Zhu, Z. Lu, and R. Xiong, Phys. Rev. B **110**, 134437 (2024).
[7] T. Kokkeler, I. Tokatly, and F. S. Bergeret, SciPost Phys. **18**, 178 (2025).
[8] M. Naka, Y. Motome, T. Miyazaki, and H. Seo, Journal of the Physical Society of Japan **94**, 083702 (2025).
[9] N. Sigales, T. Kokkeler, G. De Polsi, and S. Bergeret, arXiv preprint arXiv:2602.07779 10.48550/arXiv.2602.07779 (2026).
[10] C. Sun and J. Linder, Phys. Rev. B **108**, L140408 (2023).
[11] S. Das, D. Suri, and A. Soori, Journal of Physics: Condensed Matter **35**, 435302 (2023).
[12] R. González-Hernández, L. Šmejkal, K. Výborný, Y. Yahagi, J. Sinova, T. Jungwirth, and J. Železný, Phys. Rev. Lett. **126**, 127701 (2021).
[13] R. He, Z. Duan, B. Lei, N. Luo, J. Zeng, K.-Q. Chen, and L.-M. Tang, Phys. Rev. B **112**, 064423 (2025).
[14] A. Herasymchuk, K. B. Hallberg, E. W. Hodt, J. Linder, E. V. Gorbar, and P. Sukhachov, Phys. Rev. B **112**, L220404 (2025).
[15] K. B. Hallberg, E. W. Hodt, and J. Linder, Phys. Rev. B **111**, 174431 (2025).

[16] E. W. Hodt, A. Qaiumzadeh, and J. Linder, Phys. Rev. B **113**, 054403 (2026).

[17] R. de las Heras, T. Kokkeler, S. Ilić, I. V. Tokatly, and F. S. Bergeret, Phys. Rev. B **113**, 144516 (2026).

[18] S. Reimers, L. Odenbreit, L. Šmejkal, V. N. Strocov, P. Constantinou, A. B. Hellenes, R. Jaeschke Ubiergo, W. H. Campos, V. K. Bharadwaj, A. Chakraborty, *et al.*, Nature Communications **15**, 2116 (2024).

[19] O. Fedchenko, J. Minár, A. Akashdeep, S. W. D'Souza, D. Vasilyev, O. Tkach, L. Odenbreit, Q. Nguyen, D. Kutnyakhov, N. Wind, *et al.*, Science advances **10**, eadj4883 (2024).

[20] C. He, Z. Wen, J. Okabayashi, Y. Miura, T. Ma, T. Ohkubo, T. Seki, H. Sukegawa, and S. Mitani, Nature Communications **16**, 8235 (2025).

[21] J. Mencos, A. Badura, E. Dolan, S. Beckert, R. Gonzalez-Hernandez, I. Kounta, M. Petit, C. Guillemard, A. B. Hellenes, W. Campos, *et al.*, arXiv preprint arXiv:2512.17427 10.48550/arXiv.2512.17427 (2025).

[22] Y. Guo, J. Zhang, Z. Zhu, Y.-y. Jiang, L. Jiang, C. Wu, J. Dong, X. Xu, W. He, B. He, *et al.*, Advanced Science , 2400967 (2024).

[23] H. Chen, Z.-A. Wang, P. Qin, Z. Meng, X. Zhou, X. Wang, L. Liu, G. Zhao, Z. Duan, T. Zhang, *et al.*, Advanced Materials **37**, 2507764 (2025).

[24] S. Hayami, Y. Yanagi, and H. Kusunose, Phys. Rev. B **101**, 220403 (2020).

[25] A. B. Hellenes, T. Jungwirth, J. Sinova, and L. Šmejkal, arXiv preprint arXiv:2309.01607v3 10.48550/arXiv.2309.01607 (2023).

[26] R. D. Gonzalez Betancourt, J. Zubác, K. Geishendorf, P. Ritzinger, B. Ruuzicková, T. Kotte, J. Veleznỳ, K. Olejník, G. Springholz, B. Büchner, *et al.*, npj Spintronics **2**, 45 (2024).

[27] Y.-F. Sun, Y. Mao, Y.-C. Zhuang, and Q.-F. Sun, Phys. Rev. B **112**, 094411 (2025).

[28] W. Thomson, Proceedings of the Royal Society of London , 546 (1857).

[29] M. N. Baibich, J. M. Broto, A. Fert, F. N. Van Dau, F. Petroff, P. Etienne, G. Creuzet, A. Friederich, and J. Chazelas, Phys. Rev. Lett. **61**, 2472 (1988).

[30] G. Binasch, P. Grünberg, F. Saurenbach, and W. Zinn, Phys. Rev. B **39**, 4828 (1989).

[31] R. E. Camley and J. Barnaś, Phys. Rev. Lett. **63**, 664 (1989).

[32] M. Julliere, Physics Letters A **54**, 225 (1975).

[33] M. I. Dyakonov, Phys. Rev. Lett. **99**, 126601 (2007).

[34] S. Vélez, V. N. Golovach, A. Bedoya-Pinto, M. Isasa, E. Sagasta, M. Abadia, C. Rogero, L. E. Hueso, F. S. Bergeret, and F. Casanova, Phys. Rev. Lett. **116**, 016603 (2016).

[35] H. Nakayama, M. Althammer, Y.-T. Chen, K. Uchida, Y. Kajiwara, D. Kikuchi, T. Ohtani, S. Geprägs, M. Opel, S. Takahashi, R. Gross, G. E. W. Bauer, S. T. B. Goennenwein, and E. Saitoh, Phys. Rev. Lett. **110**, 206601 (2013).

[36] Y.-T. Chen, S. Takahashi, H. Nakayama, M. Althammer, S. T. B. Goennenwein, E. Saitoh, and G. E. W. Bauer, Phys. Rev. B **87**, 144411 (2013).

[37] C. Hahn, G. de Loubens, O. Klein, M. Viret, V. V. Naletov, and J. Ben Youssef, Phys. Rev. B **87**, 174417 (2013).

[38] M. Althammer, S. Meyer, H. Nakayama, M. Schreier, S. Altmannshofer, M. Weiler, H. Huebl, S. Geprägs, M. Opel, R. Gross, D. Meier, C. Klewe, T. Kuschel, J.-M. Schmalhorst, G. Reiss, L. Shen, A. Gupta, Y.-T. Chen, G. E. W. Bauer, E. Saitoh, and S. T. B. Goennenwein, Phys. Rev. B **87**, 224401 (2013).

[39] M. Isasa, A. Bedoya-Pinto, S. Vélez, F. Golmar, F. Sánchez, L. E. Hueso, J. Fontcuberta, and F. Casanova, Applied Physics Letters **105**, 10.1063/1.4897544 (2014).

[40] S. Meyer, M. Althammer, S. Geprägs, M. Opel, R. Gross, and S. T. Goennenwein, Applied Physics Letters **104**, 10.1063/1.4885086 (2014).

[41] S. R. Marmion, M. Ali, M. McLaren, D. A. Williams, and B. J. Hickey, Phys. Rev. B **89**, 220404 (2014).

[42] J. Kim, P. Sheng, S. Takahashi, S. Mitani, and M. Hayashi, Phys. Rev. Lett. **116**, 097201 (2016).

[43] S. Vélez, V. N. Golovach, J. M. Gomez-Perez, A. Chuvilin, C. T. Bui, F. Rivadulla, L. E. Hueso, F. S. Bergeret, and F. Casanova, Phys. Rev. B **100**, 180401 (2019).

[44] K.-i. Uchida, Z. Qiu, T. Kikkawa, R. Iguchi, and E. Saitoh, Applied Physics Letters **106**, 10.1063/1.4907546 (2015).

[45] X.-P. Zhang, F. S. Bergeret, and V. N. Golovach, Nano letters **19**, 6330 (2019).

[46] H. Nakayama, M. Althammer, Y.-T. Chen, K. Uchida, Y. Kajiwara, D. Kikuchi, T. Ohtani, S. Geprägs, M. Opel, S. Takahashi, R. Gross, G. E. W. Bauer, S. T. B. Goennenwein, and E. Saitoh, Phys. Rev. Lett. **110**, 206601 (2013).

[47] K. Maeda, Y. Fukaya, K. Yada, B. Lu, Y. Tanaka, and J. Cayao, Phys. Rev. B **111**, 144508 (2025).

[48] F. S. Bergeret and I. V. Tokatly, Phys. Rev. Lett. **110**, 117003 (2013).

[49] M. M. Vasiakin and A. S. Mel'nikov, Phys. Rev. B **111**, L100502 (2025).

[50] A. Kitz, physica status solidi (b) **10**, 455 (1965).

[51] W. Brinkman and R. Elliott, Journal of Applied Physics **37**, 1457 (1966).

[52] W. Brinkman and R. J. Elliott, Proceedings of the Royal Society of London. Series A. Mathematical and Physical Sciences **294**, 343 (1966).

[53] D. B. Litvin and W. Opechowski, Physica **76**, 538 (1974).

[54] D. B. Litvin, Acta Crystallographica Section A: Crystal Physics, Diffraction, Theoretical and General Crystallography **33**, 279 (1977).

[55] P. Liu, J. Li, J. Han, X. Wan, and Q. Liu, Phys. Rev. X **12**, 021016 (2022).

[56] Y. Jiang, Z. Song, T. Zhu, Z. Fang, H. Weng, Z.-X. Liu, J. Yang, and C. Fang, Phys. Rev. X **14**, 031039 (2024).

[57] X. Chen, J. Ren, Y. Zhu, Y. Yu, A. Zhang, P. Liu, J. Li, Y. Liu, C. Li, and Q. Liu, Phys. Rev. X **14**, 031038 (2024).

[58] Z. Xiao, J. Zhao, Y. Li, R. Shindou, and Z.-D. Song, Phys. Rev. X **14**, 031037 (2024).

[59] K. Shinohara, A. Togo, H. Watanabe, T. Nomoto, I. Tanaka, and R. Arita, Acta Crystallographica Section A: Foundations and Advances **80**, 10.1107/S2053273323009257 (2024).

[60] H. Schiff, A. Corticelli, A. Guerreiro, J. Romhányi, and P. A. McClarty, SciPost Physics **18**, 109 (2025).

[61] X. Feng and Z. Zhang, Phys. Rev. B **111**, 054520 (2025).

[62] M. B. Lifshits and M. I. Dyakonov, Phys. Rev. Lett. **103**, 186601 (2009).

[63] A. Brataas, Y. V. Nazarov, and G. E. Bauer, Physical Review Letters **84**, 2481 (2000).

[64] F. K. Dejene, N. Vlietstra, D. Luc, X. Waintal, J. Ben Youssef, and B. J. van Wees, Phys. Rev. B **91**, 100404 (2015).

[65] T. Shang, Q. Zhan, H. Yang, Z. Zuo, Y. Xie, L. Liu, S. Zhang, Y. Zhang, H. Li, B. Wang, *et al.*, Applied Physics Letters **109**, 10.1063/1.4959573 (2016).

[66] D. Hou, Z. Qiu, J. Barker, K. Sato, K. Yamamoto, S. Vélez, J. M. Gomez-Perez, L. E. Hueso, F. Casanova, and E. Saitoh, Phys. Rev. Lett. **118**, 147202 (2017).

[67] G. R. Hoogeboom, A. Aqeel, T. Kuschel, T. Palstra, and B. J. van Wees, Applied Physics Letters **111**, 10.1063/1.4997588 (2017).

[68] L. Baldrati, A. Ross, T. Niizeki, C. Schneider, R. Ramos, J. Cramer, O. Gomonay, M. Filianina, T. Savchenko, D. Heinze, A. Kleibert, E. Saitoh, J. Sinova, and M. Kläui, Phys. Rev. B **98**, 024422 (2018).

[69] Y. Cheng, S. Yu, A. S. Ahmed, M. Zhu, Y. Rao, M. Ghazisaeidi, J. Hwang, and F. Yang, Phys. Rev. B **100**, 220408 (2019).

[70] J. Fischer, M. Althammer, N. Vlietstra, H. Huebl, S. T. Goennenwein, R. Gross, S. Geprägs, and M. Opel, Phys. Rev. Appl. **13**, 014019 (2020).

[71] Y. Wu, J. Zhou, X. Shi, Y. Liu, Q. Liu, K. K. Meng, J. K. Chen, X. G. Xu, Y. Jiang, and M. Yang, Advanced Functional Materials , 2425280 (2025).

[72] J. M. Gomez-Perez, X.-P. Zhang, F. Calavalle, M. Ilyn, C. González-Orellana, M. Gobbi, C. Rogero, A. Chuvilin, V. N. Golovach, L. E. Hueso, *et al.*, Nano Letters **20**, 6815 (2020).

Appendix A: Arbitrary anisotropy of spin-relaxation

In this Appendix we provide the details of the calculation of the spin-splitter magnetoresistance, SSMR. Specifically, starting from the charge conservation and spin diffusion equations, Eqs. (1 and 2) we derive Eq. (12) for the longitudinal resistance correction and Eq. (15) for the transverse resistance in the main text. Moreover, we show how the limits of isotropic relaxation, Eqs. (14-21) in the main text, and highly anisotropic relaxation, Eq. (22) in the main text, follow directly from our general expression.

We consider a geometry in which an altermagnet carrier a current in its infinite x direction, has a boundary with air at $y = \frac{L_y}{2}$ and a boundary with an FI at $y = -\frac{L_y}{2}$. By translational invariance while μ satisfies

$$\mu = -Ex + \delta\mu(y) \ , \tag{A1}$$

where E is a scalar that corresponds to the electric field. Moreover, because of spin-relaxation, translational invariance requires that the spin chemical potential $\boldsymbol{\mu}^s$ depends only on y.

Exploiting this translational invariance, Eqs. (1) and (2) reduce to effectively one-dimensional equations. T At the boundary at $y = \frac{L_y}{2}$ both charge current and spin current are vanishing. At the boundary at $y = -\frac{L_y}{2}$ the charge current is vanishing, since we consider a ferromagnetic insulator, but the spin current satisfies Eq. (8) in the main text.

For the optimal orientation for the SSMR, in which $T_{yy} = 0$, the equations for $\delta\mu$ and μ^s are decoupled. For $\delta\mu$ we obtain

$$\partial_{yy}\delta\mu = 0 \ , \tag{A2}$$

$$\partial_{y}\delta\mu = 0 \ , \qquad (y = \pm\frac{L_y}{2}) \ . \tag{A3}$$

Thus, $\delta\mu$ is a constant, which may be set to zero by choice of the origin for the x-coordinate. For $\boldsymbol{\mu}^s$ we have the following boundary value problem

$$D\partial_{yy}\boldsymbol{\mu}^s = \frac{1}{\tau_{s\parallel}}(\boldsymbol{\mu}_s \cdot \boldsymbol{N})\boldsymbol{N} + \frac{1}{\tau_{s\perp}}\boldsymbol{N} \times (\boldsymbol{\mu}_s \times \boldsymbol{N}) \ , \tag{A4}$$

$$D\partial_{y}\boldsymbol{\mu}^s(y = \frac{L_y}{2}) = 2T_{xy}DE\boldsymbol{N} \ , \tag{A5}$$

$$D\partial_{y}\boldsymbol{\mu}^s(y = -\frac{L_y}{2}) = 2T_{xy}DE\boldsymbol{N} + D\frac{2|G_s|}{\sigma}\boldsymbol{\mu}^s - D\frac{2G_r}{\sigma}\boldsymbol{m} \times (\boldsymbol{m} \times \boldsymbol{\mu}^s) - D\frac{2G_i}{\sigma}\boldsymbol{m} \times \boldsymbol{\mu}^s. \tag{A6}$$

This is a set of three one-dimensional second order diffusion equations with constant coefficients. The bulk equation and the boundary condition at $y = \frac{L_y}{2}$ dictate that the solution can be written as

$$\boldsymbol{\mu}^s = (2T_{xy}El_{s\parallel}\frac{\sinh\frac{y}{l_{s\parallel}}}{\cosh\frac{L_y}{2l_{s\parallel}}} + C_1\frac{\cosh\frac{y-\frac{L_y}{2}}{l_{s\parallel}}}{\sinh\frac{L_y}{l_{s\parallel}}})\boldsymbol{N} + \boldsymbol{C}_2\frac{\cosh\frac{y-\frac{L_y}{2}}{l_{s\perp}}}{\sinh\frac{L_y}{l_{s\perp}}} \ , \tag{A7}$$

where $\boldsymbol{C}_2 \cdot \boldsymbol{N} = 0$ and $l_{s\parallel,\perp} = \sqrt{D\tau_{s\parallel,\perp}}$.

From this solution, the charge current in the x-direction, can be written as

$$J_x = L_y\sigma E - \frac{\sigma}{2}T_{xy}(\boldsymbol{N}\cdot\boldsymbol{\mu}^s(y=\frac{L_y}{2}) - \boldsymbol{N}\cdot\boldsymbol{\mu}^s(y=\frac{L_y}{2})) = L_y\sigma E - 2\sigma T_{xy}^2 E l_{s\parallel}\tanh\frac{L_y}{2l_{s\parallel}} + \frac{1}{2}\sigma T_{xy}C_1\tanh\frac{L_y}{2l_{s\parallel}} \ . \tag{A8}$$

Thus, the SSMR is determined by the coefficient C_1 in Eq. (A7).

To determine C_1 and $\boldsymbol{C}_2$, we consider the boundary condition at $y = -\frac{L_y}{2}$. It is convenient to make a change of basis to the following basis. We write $\boldsymbol{\mu}^s = \mu^s_m\boldsymbol{m} + \mu^s_{\perp 1}\boldsymbol{a} + \mu^s_{\perp 2}\boldsymbol{b}$, where $\boldsymbol{a},\boldsymbol{b}$ are vectors perpendicular to $\boldsymbol{m}$ such that $\boldsymbol{N} = (\boldsymbol{m}\cdot\boldsymbol{N})\boldsymbol{m} + (\boldsymbol{a}\cdot\boldsymbol{N})\boldsymbol{a}$ and $\boldsymbol{b} = \boldsymbol{m}\times\boldsymbol{a}$. Next we define the complex quantity $\mu^s_\perp = \mu^s_{\perp 1} + i\mu^s_{\perp 2}$.

In this basis, the general solution can be written as

$$\mu^s_m = (2T_{xy}El_{s\parallel}\frac{\sinh\frac{y}{l_{s\parallel}}}{\cosh\frac{L_y}{2l_{s\parallel}}} + C_1\frac{\cosh\frac{y-\frac{L_y}{2}}{l_{s\parallel}}}{\sinh\frac{L_y}{l_{s\parallel}}})\cos\phi + \mathrm{Re}(C_3)\frac{\cosh\frac{y-\frac{L_y}{2}}{l_{s\perp}}}{\sinh\frac{L_y}{l_{s\perp}}}\sin\phi \ , \tag{A9}$$

$$\mu^s_\perp = (2T_{xy}El_{s\parallel}\frac{\sinh\frac{y}{l_{s\parallel}}}{\cosh\frac{L_y}{2l_{s\parallel}}} + C_1\frac{\cosh\frac{y-\frac{L_y}{2}}{l_{s\parallel}}}{\sinh\frac{L_y}{l_{s\parallel}}})\sin\phi - (\mathrm{Re}C_3\cos\phi + i\mathrm{Im}C_3)\frac{\cosh\frac{y-\frac{L_y}{2}}{l_{s\perp}}}{\sinh\frac{L_y}{l_{s\perp}}} \ , \tag{A10}$$

where ϕ is the angle between $\boldsymbol{m}$ and $\boldsymbol{N}$, C_3 is a complex number such that $\mathrm{Re}(C_3) = \sqrt{(\boldsymbol{m}\cdot\boldsymbol{C}_2)^2 + (\boldsymbol{a}\cdot\boldsymbol{C}_2)^2}$ and $\mathrm{Im}(C_3) = \boldsymbol{b}\cdot\boldsymbol{C}_2$, while C_1 is the same real number as in Eq. (A7).

The boundary condition at $y = -\frac{L_y}{2}$ in this basis reads

$$\sigma\partial_y\mu^s_m = 2T_{xy}E\cos\phi + 2|G_s|\mu^s_m \ , \tag{A11}$$

$$\sigma\partial_y\mu^s_\perp = 2T_{xy}E\sin\phi + 2(|G_s| + G_r - iG_i)\mu^s_\perp \ . \tag{A12}$$

Now, for short-hand notation we define $G_{\parallel,\perp} = \frac{\sigma}{l_{s\parallel,\perp}}$ and $\mu^s_0 = 2T_{xy}El_{s\parallel}\tanh\frac{L_y}{2l_{s\parallel}}$. Substituting Eqs. (A9,A10) into Eqs. (A11,A12) we find

$$G_\parallel C_1\cos\phi + G_\perp\mathrm{Re}(C_3)\sin\phi = 2|G_s|\Big((\mu^s_0 - C_1\coth\frac{L_y}{2l_{s\parallel}})\cos\phi - \mathrm{Re}(C_3)\coth\frac{L_y}{2l_{s\perp}})\sin\phi\Big) \ , \tag{A13}$$

$$G_\parallel C_1\sin\phi - G_\perp C_3\cos\phi = 2(|G_s| + G_r - iG_i)\Big((\mu^s_0 - C_1\coth\frac{L_y}{2l_{s\parallel}})\sin\phi + (\mathrm{Re}(C_3)\cos\phi + i\mathrm{Im}C_3)\coth\frac{L_y}{2l_{s\perp}})\Big) \ . \tag{A14}$$

Notably, the first equation, only involves C_1 and $\mathrm{Re}(C_3)$, while the second equation may be rewritten as

$$\mathrm{Re}(C_3)\cos\phi + i\mathrm{Im}(C_3) - (\frac{G_\parallel + 2(|G_s| + G_r - G_i)\coth\frac{L_y}{l_{s\parallel}}}{G_\perp + 2(|G_s| + G_r - G_i)\coth\frac{L_y}{l_{s\perp}}})C_1 = -2\mu^s_0\sin\phi\frac{|G_s| + G_r - iG_i}{G_\perp + 2(|G_s| + G_r - G_i)\coth\frac{L_y}{l_{s\perp}}} \ . \tag{A15}$$

By taking the real part of this equation one obtains an equation that involves C_1 and $\mathrm{Re}(C_3)$. Thus, C_1 and $\mathrm{Re}(C_3)$ can be determined by the system of Eq. (A13) and the real part of (A15). The imaginary part of Eq. (A15) can then in principle be used to determine $\mathrm{Im}(C_3)$. However, since the SSMR only depends on C_1, we do not need to do so.

With this, we have reduced the problem to a set of two linear equations:

$$(G_\parallel + 2|G_s|\coth\frac{L_y}{2l_{s\parallel}})\cos\phi C_1 + (G_\perp + 2|G_s|\coth\frac{L_y}{2l_{s\perp}})\sin\phi\mathrm{Re}(C_3) = 2|G_s|\mu^s_0\cos\phi \ , \tag{A16}$$

$$\mathrm{Re}(C_3)\cos\phi - \mathrm{Re}(\frac{G_\parallel + 2(|G_s| + G_r - G_i)\coth\frac{L_y}{l_{s\parallel}}}{G_\perp + 2(|G_s| + G_r - G_i)\coth\frac{L_y}{l_{s\perp}}})C_1 = -2\mu^s_0\sin\phi\mathrm{Re}\frac{|G_s| + G_r - iG_i}{G_\perp + 2(|G_s| + G_r - G_i)\coth\frac{L_y}{l_{s\perp}}} \ . \tag{A17}$$

Introducing $\mathcal{R}(G) = \mathrm{Re}\Big(\frac{2G}{G_\perp + 2G\coth\frac{L_y}{l_{s\perp}}}\Big) = \mathrm{Re}\Big(\frac{2Gl_{s\perp}}{\sigma + 2Gl_{s\perp}\coth\frac{L_y}{l_{s\perp}}}\Big)$, this can be written as,

$$\mathrm{Re}(C_3)\sin\phi + (\frac{G_\parallel}{G_\perp} + \mathcal{R}(|G_s|)(\coth\frac{L_y}{l_{s\parallel}} - \frac{G_\parallel}{G_\perp}\coth\frac{L_y}{l_{s\perp}})C_1\cos\phi = \mu_0^s\cos\phi\mathcal{R}(|G_s|)\ , \tag{A18}$$

$$\mathrm{Re}(C_3)\cos\phi - (\frac{G_\parallel}{G_\perp} + \mathcal{R}(|G_s| + G_{\uparrow\downarrow})(\coth\frac{L_y}{l_{s\parallel}} - \frac{G_\parallel}{G_\perp}\coth\frac{L_y}{l_{s\perp}})C_1\sin\phi = -\mu_0^s\mathcal{R}(|G_s| + G_{\uparrow\downarrow})\sin\phi\ , \tag{A19}$$

Eliminating $\mathrm{Re}(C_3)$, we find

$$C_1 = \mu_0^s\frac{\mathcal{R}(|G_s|) + (\mathcal{R}(|G_s| + G_{\uparrow\downarrow}) - \mathcal{R}(|G_s|))\sin^2\phi}{\frac{l_{s\perp}}{l_{s\parallel}} + \Big(\mathcal{R}(|G_s|) + (\mathcal{R}(|G_s| + G_{\uparrow\downarrow}) - \mathcal{R}(|G_s|))\sin^2\phi\Big)(\coth\frac{L_y}{l_{s\parallel}} - \frac{l_{s\perp}}{l_{s\parallel}}\coth\frac{L_y}{l_{s\perp}})}\ . \tag{A20}$$

Next, we may exploit

$$\begin{aligned}\mathcal{R}(|G_s| + G_{\uparrow\downarrow}) - \mathcal{R}(|G_s|) &= \mathrm{Re}\frac{-2|G_s|(\sigma + 2(|G_s| + G_{\uparrow\downarrow})l_{s\perp}\coth\frac{L_y}{l_{s\perp}}) + 2(|G_s| + G_{\uparrow\downarrow})(\sigma + 2|G_s|l_{s\perp}\coth\frac{L_y}{l_{s\perp}})}{(\sigma + 2|G_s|l_{s\perp}\coth\frac{L_y}{l_{s\perp}})(\sigma + 2(|G_s| + G_{\uparrow\downarrow})l_{s\perp}\coth\frac{L_y}{l_{s\perp}})} \\ &= \mathrm{Re}\frac{1}{\sigma + 2|G_s|l_{s\perp}\coth\frac{L_y}{l_{s\perp}}}\frac{G_{\uparrow\downarrow}l_{s\perp}}{1 + 2\frac{|G_s| + G_{\uparrow\downarrow}}{\sigma}l_{s\perp}\coth\frac{L_y}{l_{s\perp}}} = \frac{2\bar{G}l_{s\perp}}{\sigma + 2G_s l_{s\perp}\coth\frac{L_y}{l_{s\perp}}}\ ,\end{aligned} \tag{A21}$$

where we define the effective conductance

$$\bar{G} = \mathrm{Re}\frac{G_{\uparrow\downarrow}}{1 + 2\frac{|G_s| + G_{\uparrow\downarrow}}{\sigma}l_{s\perp}\coth\frac{L_y}{l_{s\perp}}}\ . \tag{A22}$$

We may now rewrite C_1 as

$$C_1 = \mu_0^s\frac{2(|G_s| + \bar{G}\sin^2\phi)l_{s\perp}}{\frac{l_{s\perp}}{l_{s\parallel}}(\sigma + 2G_s l_{s\perp}\coth\frac{L_y}{l_{s\perp}}) + 2(|G_s| + \bar{G}\sin^2\phi)(\coth\frac{L_y}{l_{s\parallel}} - \frac{l_{s\perp}}{l_{s\parallel}}\coth\frac{L_y}{l_{s\perp}})} \tag{A23}$$

$$= \mu_0^s\frac{2\frac{l_{s\parallel}}{\sigma}(|G_s| + \bar{G}\sin^2\phi)}{1 + \frac{2|G_s|l_{s\perp}}{\sigma}\coth\frac{L_y}{l_{s\perp}} + 2(|G_s| + \bar{G}\sin^2\phi)(\frac{l_{s\parallel}}{\sigma}\coth\frac{L_y}{l_{s\parallel}} - \frac{l_{s\perp}}{\sigma}\coth\frac{L_y}{l_{s\perp}})} \tag{A24}$$

$$= \mu_0^s\frac{\frac{l_{s\parallel}}{\sigma}2(|G_s| + \bar{G}\sin^2\phi)}{1 + \frac{2|G_s|l_{s\parallel}}{\sigma}\coth\frac{L_y}{l_{s\parallel}} + 2(\frac{l_{s\parallel}}{\sigma}\coth\frac{L_y}{l_{s\parallel}} - \frac{l_{s\perp}}{\sigma}\coth\frac{L_y}{l_{s\perp}})\bar{G}\sin^2\phi}\ . \tag{A25}$$

As discussed before, C_1 determines the SSMR strength, through Eq. (A8). Indeed, Eq. (A8) implies

$$\delta J = J - \sigma L_y E = -T_{xy}\sigma(\mu_0^s - \frac{1}{2}\tanh\frac{L_y}{2l_{s\parallel}}C_1)\ . \tag{A26}$$

Substituting Eq. (A23) into Eq. (A26) and exploiting that $2\coth\frac{L_y}{l_{s\parallel}} - \tanh\frac{L_y}{2l_{s\parallel}} = \coth\frac{L_y}{2l_{s\parallel}}$, we find

$$\delta J = -T_{xy}\mu_0^s(1 - \frac{1}{2}\mu_0^s\frac{2\frac{l_{s\parallel}}{\sigma}\tanh\frac{L_y}{2l_{s\parallel}}(|G_s| + \bar{G}\sin^2\phi)}{1 + \frac{2|G_s|l_{s\parallel}}{\sigma}\coth\frac{L_y}{l_{s\parallel}} + 2(\frac{l_{s\parallel}}{\sigma}\coth\frac{L_y}{l_{s\parallel}} - \frac{l_{s\perp}}{\sigma}\coth\frac{L_y}{l_{s\perp}})\bar{G}\sin^2\phi} \tag{A27}$$

$$= -T_{xy}\sigma\mu_0^s\frac{1 + \frac{|G_s|l_{s\parallel}}{\sigma}\coth\frac{L_y}{2l_{s\parallel}} + (\frac{l_{s\parallel}}{\sigma}\coth\frac{L_y}{2l_{s\parallel}} - 2\frac{l_{s\perp}}{\sigma}\coth\frac{L_y}{l_{s\perp}})\bar{G}\sin^2\phi}{1 + \frac{2|G_s|l_{s\parallel}}{\sigma}\coth\frac{L_y}{l_{s\parallel}} + 2(\frac{l_{s\parallel}}{\sigma}\coth\frac{L_y}{l_{s\parallel}} - \frac{l_{s\perp}}{\sigma}\coth\frac{L_y}{l_{s\perp}})\bar{G}\sin^2\phi}\ , \tag{A28}$$

so that, substituting $\mu_0^s = 2T_{xy}El_{s\parallel}\tanh\frac{L_y}{2l_{s\parallel}}$ and using $\frac{\delta J}{J} = -\frac{\Delta\rho}{\rho}$, we find

$$\frac{\Delta\rho}{\rho_L} = 2T_{xy}^2\frac{l_{s\parallel}}{L_y}\tanh\frac{L_y}{2l_{s\parallel}}\frac{1 + \frac{|G_s|l_{s\parallel}}{2\sigma}\coth\frac{L_y}{2l_{s\parallel}} + (\frac{l_{s\parallel}}{2\sigma}\coth\frac{L_y}{2l_{s\parallel}} - \frac{l_{s\perp}}{\sigma}\coth\frac{L_y}{l_{s\perp}})\bar{G}\sin^2\phi}{1 + \frac{|G_s|l_{s\parallel}}{\sigma}\coth\frac{L_y}{l_{s\parallel}} + (\frac{l_{s\parallel}}{\sigma}\coth\frac{L_y}{l_{s\parallel}} - \frac{l_{s\perp}}{\sigma}\coth\frac{L_y}{l_{s\perp}})\bar{G}\sin^2\phi}\ . \tag{A29}$$

Multiplying both sides with $\rho_L = \sigma^{-1}$, we recover Eq. (12) in the main text.

Moreover, we have

$$J_z = \int_{-\frac{L_y}{2}}^{\frac{L_y}{2}} -\sigma(\partial_z \nu + T_{yz}\boldsymbol{N}\cdot\partial_y \boldsymbol{\mu}^s + T_{xz}\boldsymbol{N}\cdot\partial_x \boldsymbol{\mu_s}) = \frac{T_y}{T_{xz}}\delta J \ . \tag{A30}$$

Therefore, we have

$$\rho_T = \frac{T_{yz}}{T_{xy}}\Delta\rho_L \ . \tag{A31}$$

This corresponds to Eq. (15) in the main text.

We may now also analyse how the special cases, isotropic relaxation, Eqs. (14-21) in the main text, and highly anisotropic relaxation, Eq. (22) in the main text, follow directly from this expression. First consider the limit of isotropic relaxation, i.e. $l_{s\parallel} = l_{s\perp} = l_s$. In that case $(\frac{l_{s\parallel}}{\sigma}\coth\frac{L_y}{l_{s\parallel}} - \frac{l_{s\perp}}{\sigma}\coth\frac{L_y}{l_{s\perp}}) \to 0$ and $(\frac{l_{s\parallel}}{2\sigma}\coth\frac{L_y}{2l_{s\parallel}} - \frac{l_{s\perp}}{\sigma}\coth\frac{L_y}{l_{s\perp}}) \to \frac{l_s}{\sigma}\coth\frac{L_y}{2l_s} - 2\frac{l_s}{\sigma}\coth\frac{L_y}{l_s} = -\frac{l_s}{\sigma}\tanh\frac{L_y}{2l_s}$, so that Eq. (A29) gives

$$\Delta\rho_L = \frac{2T_{xy}^2 l_s}{\sigma L_y}\tanh\frac{L_y}{2l_s}\frac{\sigma + |G_s| l_s \coth\frac{L_y}{l_s} - \bar{G} l_s \tanh\frac{L_y}{2l_s}\sin^2\phi}{\sigma + |G_s| l_S \coth\frac{L_y}{l_s}} \tag{A32}$$

$$= \frac{2T_{xy}^2 l_s}{\sigma L_y}\frac{\sigma\tanh\frac{L_y}{2l_s} + |G_s| l_s}{\sigma + |G_s| l_S \coth\frac{L_y}{l_s}} - \frac{2T_{xy}^2 l_s}{\sigma L_y}\frac{\bar{G} l_s \tanh^2\frac{L_y}{2l_s}}{\sigma + |G_s| l_S \coth\frac{L_y}{l_s}}\sin^2\phi \ . \tag{A33}$$

Identifying $\sin^2\phi = 1 - (\boldsymbol{m}\cdot\boldsymbol{N})^2$, and labelling the first term $\Delta\rho_0$ and the second term $\Delta\rho_1$, we recover Eqs. (14-21) in the main text.

Next, consider the limit of highly anisotropic relaxation in which case $l_{s\perp} \to 0$. so that also $l_{s\perp}\coth\frac{L_y}{l_{s\perp}} \to 0$ In this limit $\bar{G} = G_r$. Moreover, since in realistic junctions $|G_s| \ll G_r$, in the main text we set $G_s \to 0$

In that case Eq. (A29) becomes

$$\Delta\rho_L = \frac{2T_{xy}^2 l_s}{\sigma L_y}\tanh\frac{L_y}{2l_{s\parallel}}\frac{\sigma + G_r l_{s\parallel}\coth\frac{L_y}{2l_{s\parallel}}\sin^2\phi}{\sigma + 2G_r l_{s\parallel}\coth\frac{L_y}{l_{s\parallel}}\sin^2\phi} \ . \tag{A34}$$

Again identifying $\sin^2\phi = 1 - (\boldsymbol{m}\cdot\boldsymbol{N})^2$, we obtain Eq. (22) in the main text.

Appendix B: Antiferromagnets

To disentangle the effects of altermagnetism and spin-orbit coupling it is important to compare the SSMR with the SMR effect in antiferromagnets. To study the SMR effect in antiferromagnets, one actually has to resort to diffusion equations that incorporate both magnetism and spin-orbit coupling, which leads to a whole range of terms, such as relaxation and an anisotropic spin-Hall tensor.

However, to lowest order, we may consider the diffusion equations for an antiferromagnet [7], which is the same as for altermagnets but with $T_{jk} = K_{jk} = 0$ due to the absence of spin-splitting, and add an isotropic spin-Hall tensor $\theta\varepsilon_{jkl}$. Indeed, any other spin-to-charge conversion effects are of higher order in quasiclassics and therefore small.

We choose the current direction to be $\hat{x}$ and the normal along y. Since there are now three directions in spin space $(\boldsymbol{n}\times\boldsymbol{j}, \boldsymbol{m}, \boldsymbol{N})$ general expressions become rather expansive. We therefore decide to linearize in $G_{i,r,s}$ for illustrative purposes.

Like in the discussion of the influence of relaxation in altermagnets, we focus on two limits, relaxation due to magnetic impurities dominates over the Dyakonov-Perel type of mechanism, and the other way around.

In the former case the spin-relaxation tensor is isotropic, $l_{s\parallel} = l_{s\perp} = l_s$. Since in the normal state magnetism-related relaxation is indistinguishable from relaxation due to SOC, the equations in this case are just those of the original SMR theory [36]. To lowest order in $G_{i,r,s}$, the spin accumulation reads

$$\boldsymbol{z}\cdot\boldsymbol{\mu}^s = 2\theta_{xyz}El_s\Big[\frac{\sinh\frac{y}{l_s}}{\cosh\frac{L_y}{2l_s}} + 2\tanh\frac{L_y}{2l_s}\frac{\cosh\frac{y-\frac{L_y}{2}}{l_s}}{\sinh\frac{L_y}{l_s}}\Big(\frac{|G_s|l_s}{\sigma} + \frac{G_r l_s}{\sigma}(1-\boldsymbol{z}\cdot\boldsymbol{m})^2\Big)\Big] , \tag{B1}$$

and the currents are given by

$$\begin{aligned} J_x &= L_y\sigma E - \frac{1}{2}\sigma\theta_{yxz}\int_{-\frac{L_y}{2}}^{\frac{L_y}{2}} dy\partial_y(\boldsymbol{z}\cdot\boldsymbol{\mu}^s) \\ &= L_y\sigma E + 2\theta_{xyz}^2\sigma El_s\tanh\frac{L_y}{2l_s} - 2\theta_{xyz}^2\sigma E\tanh^2\frac{L_y}{2l_s}\Big(\frac{|G_s|}{\sigma} + G_r(1-(\boldsymbol{z}\cdot\boldsymbol{m})^2)\Big) . \end{aligned} \tag{B2}$$

Note the sign difference compared to the SSMR case is purely due to $\theta_{yxz} = -\theta_{xyz}$. Consider the case in which the relaxation for spins perpendicular to the axis is much stronger than for those parallel to it. In this case we obtain $\boldsymbol{\mu}^s \approx \mu^s\boldsymbol{N}$ and we have

$$\partial_{yy}\mu^s = \frac{1}{l_{s\parallel}^2}\mu^s . \tag{B3}$$

$$\partial_y\mu^s = 2\theta_{xyz}E\boldsymbol{N}\cdot\boldsymbol{z} , \qquad y = \frac{L_y}{2} . \tag{B4}$$

$$\begin{aligned} \partial_y\mu^s &= 2\theta_{xyz}E\boldsymbol{N}\cdot\boldsymbol{z} + 2(\frac{|G_s|}{\sigma} - \frac{G_r}{\sigma}\boldsymbol{N}\cdot(\boldsymbol{m}\times(\boldsymbol{m}\times\boldsymbol{N})) - G_i\boldsymbol{N}\cdot(\boldsymbol{m}\times\boldsymbol{N}))\mu^s \\ &= 2\theta_{xyz}E\boldsymbol{N}\cdot\boldsymbol{z} + 2(\frac{|G_s|}{\sigma} + \frac{G_r}{\sigma}(1-(\boldsymbol{N}\cdot\boldsymbol{m})^2)\mu^s , \qquad y = -\frac{L_y}{2} . \end{aligned} \tag{B5}$$

The solution to this equation is

$$\mu^s = \boldsymbol{N}\cdot\boldsymbol{z}2\theta_{xyz}E\Big[\frac{\sinh\frac{y}{l_{s\parallel}}}{\cosh\frac{L_y}{2l_{s\parallel}}} + l_{s\parallel}\tanh\frac{L_y}{2l_{s\parallel}}\frac{\cosh\frac{y-\frac{L_y}{2}}{l_{s\parallel}}}{\sinh\frac{L_y}{l_s}}\Big(\frac{|G_s|l_{s\parallel} + G_r l_{s\parallel}(1-(\boldsymbol{N}\cdot\boldsymbol{m})^2)}{\sigma + (|G_s|l_{s\parallel} + G_r l_{s\parallel}(1-(\boldsymbol{N}\cdot\boldsymbol{m})^2))\coth\frac{L_y}{l_{s\parallel}}}\Big)\Big] . \tag{B6}$$

With this, we have

$$\begin{aligned} J_x = L_y\sigma E - \frac{1}{2}\sigma\theta_{yxz}\int_{-\frac{L_y}{2}}^{\frac{L_y}{2}} dy\partial_y(\boldsymbol{z}\cdot\boldsymbol{N}\mu^s) &= L_y\sigma E + 2\theta_{xyz}^2\sigma El_s\tanh\frac{L_y}{2l_s}(\boldsymbol{N}\cdot\boldsymbol{z})^2 \\ - 2\theta_{xyz}^2\sigma(\boldsymbol{N}\cdot\boldsymbol{z})^2E\tanh^2\frac{L_y}{2l_s}\Big(&\frac{|G_s|l_{s\parallel} + G_r l_{s\parallel}(1-(\boldsymbol{N}\cdot\boldsymbol{m})^2)}{\sigma + (|G_s|l_{s\parallel} + G_r l_{s\parallel}(1-(\boldsymbol{N}\cdot\boldsymbol{m})^2))\coth\frac{L_y}{l_{s\parallel}}}\Big) . \end{aligned} \tag{B7}$$

Meanwhile the transverse current is

$$
\begin{aligned}
J_z &= \int_{-\frac{L_y}{2}}^{\frac{L_y}{2}} dy - \sigma(\partial_z \mu + \theta \varepsilon_{yzx} \partial_y \mu^s \boldsymbol{N} \cdot \boldsymbol{x} + \theta \varepsilon_{xzy} \partial_x \mu^s \boldsymbol{N} \cdot \boldsymbol{y}) \\
&= \int_{-\frac{L_y}{2}}^{\frac{L_y}{2}} dy - \sigma \theta_{xyz} \boldsymbol{N} \cdot \boldsymbol{x} \partial_y \mu^s \\
&= \frac{\boldsymbol{N} \cdot \boldsymbol{x}}{\boldsymbol{N} \cdot \boldsymbol{z}} (J_x - L_y \sigma E) \ . \qquad \text{(B8)}
\end{aligned}
$$

We thus see that SMR in antiferromagnets has features of both the usual SMR and of the SSMR. Indeed, like the SSMR, the resistance depends on the angle between the magnetization of the FI and the Néel vector and the transverse and longitudinal resistivities have the same angle dependence. Moreover, like in SSMR, the anisotropic relaxation leads to an anharmonicity due to the appearance of $1 - (\boldsymbol{N} \cdot \boldsymbol{m})^2$ not only in the numerator, but also in the denominator.

On the other hand, the sign of SMR for antiferromagnets is the same as for the SMR for normal metals, it is minimized along a specific axis and maximized along a plane. Moreover, this sign difference means that the anharmonicity leads to a widening of the peaks and tightening of the dips, opposite to the SSMR. The magnitude of the effect is relativistic and it is determined by the relative direction of $\boldsymbol{N}$ and $\boldsymbol{z}$. This shows that the SMR in antiferromagnets can be distinguished both from the usual SMR and from the SSMR. In the case spin-relaxation is only slightly anisotropic the MR depends on both $\boldsymbol{m} \cdot \boldsymbol{N}$ and $\boldsymbol{m} \cdot \boldsymbol{z}$. This case can therefore be clearly distinguished from conventional SMR and SSMR as well.